

# Improved serpentine laminating micromixer with enhanced local advection

Jang Min Park · Dong Sung Kim · Tae Gon Kang ·  
Tai Hun Kwon

Received: 18 January 2007 / Accepted: 2 July 2007 / Published online: 14 August 2007  
© Springer-Verlag 2007

**Abstract** It is a complicated task to achieve high level of mixing inside a microchannel because the flow is characterized by low Reynolds number ( $Re$ ). Recently, the serpentine laminating micromixer (SLM) was reported to achieve efficient chaotic mixing by introducing “F”-shape mixing units successively in two layers such that two mixing mechanisms, namely splitting/recombination and chaotic advection, enhance the mixing performance in combination. The present paper proposes an improved serpentine laminating micromixer (ISLM) with a novel redesign of the “F”-shape mixing unit: reduced cross-sectional area at the recombination region locally enhances advection effect which helps better vertical lamination, resulting in improved mixing performance. Flow characteristics and mixing performances of SLM and ISLM are investigated numerically and verified experimentally. Numerical analysis system is developed based on a finite element method and a colored particle tracking method, while mixing entropy is adopted as a mixing measure. Numerical analysis result confirms enhanced vertical lamination performance and consequently improved mixing performance of ISLM. SLM and ISLM were fabricated by polydimethylsiloxane (PDMS) casting against SU-8 patterned masters. Mixing performance is observed by

normalized purple color intensity change of phenolphthalein along the downchannel. Flow characteristics of SLM and ISLM are investigated by tracing the purple interface of two streams via optical micrograph. The normalized mixing intensity behavior confirms improved mixing performance of ISLM, which is consistent with numerical analysis result.

**Keywords** Micromixer · Chaotic advection · Lamination

## 1 Introduction

Microfluidic systems are widely utilized in miniaturized analytical systems such as micro-total-analysis systems and lab-on-a-chip systems for biological analysis, chemical synthesis and clinical diagnostics (Manz et al. 1990; Verpoorte 2002; Chow 2002). These systems usually require rapid mixing (Verpoorte et al. 2002; Chow 2002). However, mixing inside the microchannel is a difficult task to accomplish because the flow is characterized by low Reynolds number ( $Re = Vd/\nu < 100$ , where  $V$  is the average flow speed,  $d$  is the length scale of the channel and  $\nu$  is the fluid kinematic viscosity). Recently, various mixing mechanisms and micromixers have been proposed to achieve efficient mixing inside the microchannels (Branebjerg et al. 1996; Schwesinger et al. 1996; Liu et al. 2000; Lee et al. 2001; Stroock et al. 2002; Kim et al. 2004, 2005).

One promising mixing mechanism is to generate chaotic behavior of the materials (Aref and Balachandar 1986; Ottino 1989). For this purpose, one can introduce time-periodic perturbations such as hydrodynamic pressure on the microchannel flow in an active manner (Lee et al. 2001). On the other hand, one can utilize the geometrical

J. M. Park · T. G. Kang · T. H. Kwon (✉)  
Department of Mechanical Engineering,  
Pohang University of Science and Technology,  
San 31 Hyoja-dong Nam-Gu, Pohang,  
Gyeongbuk 790-784, South Korea  
e-mail: thkwon@postech.ac.kr

D. S. Kim  
School of Mechanical Engineering,  
Chung-Ang University, 221 Heukseok-dong Dongjak-gu,  
Seoul 156-756, South Korea

shape of the microchannel to achieve the chaotic behavior passively, and passive mixing is advantageous in terms of practical application purposes. For an example of the passive mixing, Liu et al. (2000) fabricated the three-dimensional serpentine microchannel by which an efficient stirring effect can be generated depending on the  $Re$ . Stroock et al. (2002) obtained helical flow using oblique ridges on the floor of the microchannel, and designed chaotic micromixer referred to as the staggered herringbone mixer by patterning grooves on the floor of the microchannel. In addition, geometrical perturbations in a periodic manner on the flow field can induce stretching and folding of the material elements, resulting in chaotic mixing (Ottino 1989; Kim and Kwon 1996; Hwang and Kwon 2000; Kim et al. 2004).

As an efficient mixing mechanism, splitting/recombination, i.e. lamination also helps rapid mixing by increasing interfacial area exponentially. The multi-layer lamination can be realized by guiding two fluids in such a way that they are added in horizontal plane, divided in vertical direction and reunited in horizontal plane. For example, Branebjerg et al. (1996) introduced a “separation plate” between microchannels which were wet etched into glass and silicon, and thereby multi-layer lamination was achieved resulting in fast mixing in laminar flow regime. Schwesinger et al. (1996) arranged fork-shaped mixing elements in two layers by bulk silicon wet etching, and they obtained relatively high level of mixing performance without the separation wall. Recently, Kim et al. (2005) developed efficient chaotic micromixer, the serpentine laminating micromixer (SLM), which combined two mixing mechanisms, i.e. splitting/recombination and chaotic advection. It might be mentioned that the SLM is advantageous in terms of practical application due to its mass producible simple design with comparable mixing performance (Kim et al. 2005, 2006).

Performance of the micromixer depends mostly on the channel geometry. Therefore, a novel design concept based on a clear understanding of the flow characteristics inside the microchannel is essential for the development of efficient micromixer. In this regard, recent flow analysis system by means of computational fluid dynamics (CFD) can provide a promising method for designing an efficient micromixer. For example, Byrde and Sawley (1999) obtained optimal twist angle of the Kenics static mixer (in this case, not micromixer) by CFD simulations. Schönfeld et al. (2004) derived optimized design for almost ideal realization of split and recombine (SAR) mixing from a detailed inspection of multi-lamination via the CFD simulation, and verified experimentally the mixing performance of so optimized micromixer.

According to CFD simulation on the SLM, it was found that vertical lamination is better achieved with the help of

the advection as  $Re$  increases (Kim et al. 2005). Kim et al. (2005) also noted that the channel aspect ratio at the recombination region would be one of the most important design parameters. In this regard, the present study proposes an improved serpentine laminating micromixer (hereinafter denoted by ISLM), which is developed to enhance the vertical lamination by introducing high local advection in the recombination region. The present paper describes the design of the ISLM and reports both experimental and numerical investigations of SLM and ISLM.

## 2 Design

The geometry at the recombination region of the SLM is modified in a “simple” manner to realize efficient vertical lamination.

The original design of the SLM is represented in Fig. 1a. By introducing “F”-shape mixing units successively in two layers, the SLM is aimed to combine the splitting/recombination and chaotic advection in a simple and mass producible design. Figure 1b schematically indicates the mixing mechanism by successive vertical laminations. Chaotic advection is generated via three-dimensional serpentine stream path when provided sufficient inertia effect, while splitting/recombination regions drive two fluids into vertical lamination mode. One notable feature of the SLM is that the advection effect due to the serpentine path design acts favorably toward the vertical lamination as  $Re$  increases (for more details about the SLM, refer to Kim

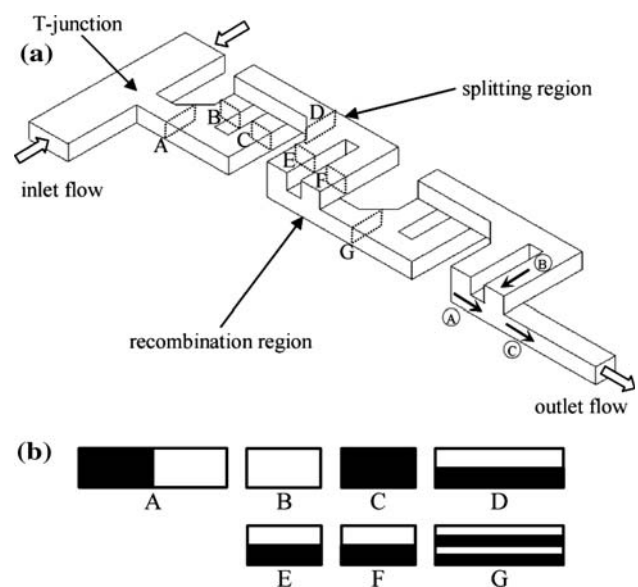
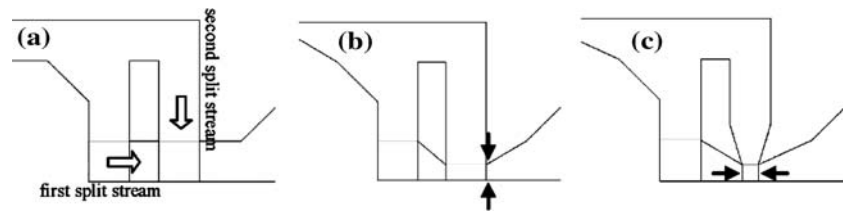


**Fig. 1** Schematic diagrams of **a** the original SLM and **b** conceptual cross-sectional mixing behaviors of the ideal vertical lamination at each indicated position

**Fig. 2** Detailed geometries (*top-view*) at the recombination region of the **a** original SLM, **b** NDI ISLM and **c** NDII ISLM



et al. 2005). In low  $Re$  regime, flow field is developed regularly along the channel geometry and thus lamination performance is determined by the channel geometry. However, as  $Re$  increases, advection affects the flow field and consequently lamination behavior can be changed depending on the  $Re$ , which may be referred to as “advection dependent lamination”. This kind of dependency of lamination on the advection effect can also be found in the SAR micromixer by Schönfeld et al. (2004); in this case, in contrast, secondary flow due to inertia effect disturbs the uniform development of lamination as  $Re$  increases.

The new improved design in this work was inspired by the feature of the SLM, i.e. “advection dependent lamination”. Two split streams should be combined in a vertical direction at the recombination region to accomplish efficient lamination, as indicated in D in Fig. 1b. However, driving two streams in a vertical direction within the flow field, in which horizontal flow is much more dominant than vertical flow due to the thin layer geometry as most situations inside the microfluidic chips are, requires sufficient advection effect to generate vertical flow. In other words, two streams should be driven in a vertical direction by high advection at the recombination region to achieve efficient vertical lamination. In this regard, one might increase the flow rate, i.e.  $Re$ . However, advection effect can also be manipulated by adjusting the micro-channel geometry, and it would be desirable if one can achieve efficient lamination irrespective of  $Re$  by enhancing advection locally via simple modification of the geometry. With this in mind, two kinds of modifications over the original design of the “F”-shape mixing unit (Fig. 2a) could be conceived to attain efficient vertical lamination as depicted in Fig. 2b, c:

- (1) New Design I (hereinafter denoted by NDI) introducing a narrower width in the zone entering the recombination region from the first split stream in the same layer (i.e. A to C in Fig. 1a), as indicated in Fig. 2b,
- (2) New Design II (hereinafter denoted by NDII), in addition to the modification in NDI, also reducing the width in the zone entering the recombination region from the second split stream in the other layer (i.e. B to C in Fig. 1a), as indicated in Fig. 2c.

The NDI is to increase the advection effect in the first split stream in the recombination region, while the NDII is designed to increase the advection in the second split stream as well as the first one. (One could suggest another possible modification where increased advection is introduced in only the second split stream. But this option was ruled out in this study since this modification is not so effective as the NDI and NDII.)

Since the original design of the SLM has an even cross-sectional area through the recombination region (Fig. 2a), flow rate should be increased to obtain higher advection effect for enhanced vertical lamination. However, in the cases of ISLMs with the NDI and NDII, “locally” high advection effect can be generated at the recombination region due to reduced channel width, i.e. cross-sectional area, for the same flow rate while maintaining the pressure drop in the similar level of the original SLM.

### 3 Numerical analysis method

Numerical analysis system is developed based on a finite element method and a colored particle tracking method to investigate the flow characteristics and the mixing performances of the original SLM and improved designs (NDI and NDII) of the ISLM (Kang and Kwon 2004).

Flow field analysis is conducted on periodic mixing units represented in Fig. 3 instead of the entire domain of micromixers because the velocity field inside the micromixer, which is composed of periodically arranged mixing units, is developed in a spatially periodic fashion. From the flow field analysis results, one can obtain the particle trajectory along the downchannel via time integration of the velocity. Governing equations for steady state incompressible flow as represented in Eq. 1 is considered for the computational domain  $\Omega$  (Fig. 3).  $\rho$  is the density,  $\underline{u}$  is the velocity vector,  $p$  is the hydrostatic pressure and  $\underline{D}$  is the rate of deformation tensor. No-slip boundary condition at the channel wall ( $\Gamma_w$ ), and traction boundary condition at the inlet and the outlet ( $\Gamma_i$  and  $\Gamma_o$ , respectively, in Fig. 3) as represented in Eq. 2 are applied (Kang and Kwon 2004).  $\Delta p$  is the pressure drop developed in one period of mixing unit,  $\underline{t}$  and  $\underline{n}$  are traction vector and outward surface normal vector, respectively. Inertia effect is included in the momentum balance equation to examine

the effect of  $Re$  on the mixing performance. In order to consider the periodic condition of the mixing unit, velocities at the inlet and outlet are constrained to be identical as represented in Eq. 3. The stabilized finite element formulation for governing equations and boundary conditions represented in Eqs. 1–3 can be stated as Eq. 4 where  $\underline{v}$  and  $q$  are weighting functions for the velocity and pressure, respectively,  $\tau$  and  $\delta$  are stabilization parameters (Hughes et al. 1989; Franca and Frey 1992).  $\lambda$  is the Lagrange multiplier introduced to consider periodic constraint in the finite element formulation and  $\varphi$  is corresponding weighting function (Kang and Kwon 2004). Computational domains, represented in Fig. 3, are discretized by cubic elements where tri-linear interpolations are employed for velocity and pressure fields.

$$\begin{cases} \rho(\underline{u} \cdot \nabla)\underline{u} + \nabla p - \nabla \cdot (2\mu\underline{D}) = \underline{0} \\ \nabla \cdot \underline{u} = 0 \end{cases} \quad (1)$$

$$\begin{cases} \underline{u} = 0 & \text{on } \Gamma_w \\ \underline{t} = -\Delta p \underline{n} + 2\mu\underline{D} \cdot \underline{n} & \text{on } \Gamma_i \\ \underline{t} = 2\mu\underline{D} \cdot \underline{n} & \text{on } \Gamma_o \end{cases} \quad (2)$$

$$\underline{u}_{in} = \underline{u}_{out} \quad (3)$$

$$\begin{aligned} & \int_{\Omega} 2\mu\underline{D}(\underline{u}) : \underline{D}(\underline{v}) d\Omega + \int_{\Omega} \rho(\underline{u} \cdot \nabla)\underline{u} \cdot \underline{v} d\Omega - \int_{\Omega} p(\nabla \cdot \underline{v}) d\Omega \\ & + \int_{\Omega} q(\nabla \cdot \underline{u}) d\Omega + \sum_K \int_{\Omega_K} (\nabla \cdot \underline{u}) \delta(\nabla \cdot \underline{v}) d\Omega_K \\ & + \sum_K \int_{\Omega_K} (\rho \underline{u} \cdot \nabla \underline{u} + \nabla p - \nabla \cdot [2\mu\underline{D}(\underline{u})]) \\ & \cdot \tau (\rho \underline{u} \cdot \nabla \underline{v} + \nabla q - \nabla \cdot [2\mu\underline{D}(\underline{v})]) d\Omega_K \\ & + \sum [\varphi(\underline{u}_{in} - \underline{u}_{out}) + \lambda(\underline{v}_{in} - \underline{v}_{out})] = \int_{\Gamma_i \cup \Gamma_o} \underline{t} \cdot \underline{v} d\Gamma \end{aligned} \quad (4)$$

Two species of red and blue colored particles are introduced at the inlet of the first mixing unit as shown in Fig. 3a. By tracking the trajectories of the colored particles, one can visualize the mixing performance inside the micromixer. It might be mentioned that these particles are passive: neither do they interact with each other nor do they exhibit diffusion via random motion; they flow only along the streamline. Trajectories of the particles are obtained by given velocities of particles from the flow analysis. For quantitative measure of the mixing performance, mixing entropy is evaluated from the colored particle distribution in the cross-section at the outlet ( $\Gamma_o$ ) of the mixing unit per period (Kang and Kwon 2004; Camesasca et al. 2005). The mixing entropy ( $S$ ) for

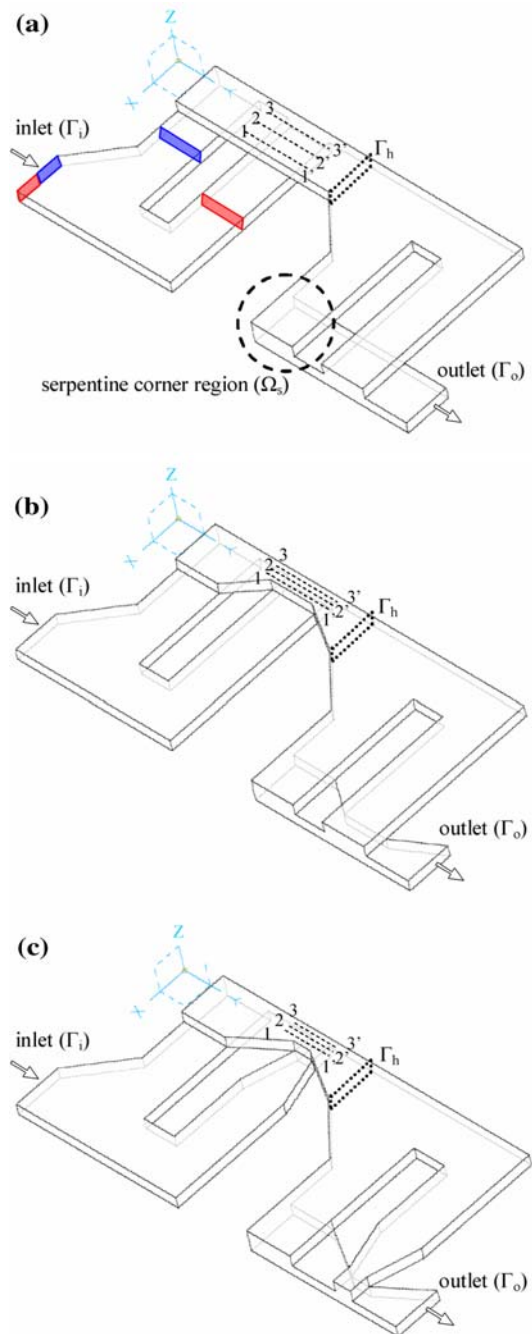


**Fig. 3** Geometries ( $\Omega$ ) of the periodic mixing units of the **a** original SLM, **b** NDI ISLM and **c** NDII ISLM used in numerical analysis. Thickness of the microchannel is 60  $\mu\text{m}$ . Numbers of finite elements are 300,600, 309,600 and 319,200, numbers of nodes are 331,669, 341,809 and 352,417 for original SLM, NDI and NDII ISLM, respectively

$N_s$  (number of species to be mixed, two in the present study) species of particles distributed in the cross-sectional area divided by  $N_c$  (number of rectangular cells constituting the cross-section, 600 in the present study)



rectangular cells is represented as follows (Kang and Kwon 2004; Camesasca et al. 2005):

$$S = - \sum_{c=1}^{N_c} P_c \sum_{s=1}^{N_s} P_{s,c} \ln P_{s,c} \quad (5)$$

where  $c$  and  $s$  are indices for cell and species, respectively.  $P_c$  is the probability that a particle is in cell  $c$  irrespective of species, while  $P_{s,c}$  is the probability that species of particle inside cell  $c$  is  $s$ . According to this definition, maximum value of the mixing entropy should be  $\ln N_s$ , when  $N_s$  species of particles are distributed uniformly over all cells (in this case,  $P_c = 1/N_c$  and  $P_{s,c} = 1/N_s$ ).

In the present study, increasing trends of the normalized mixing entropy through the five periodic mixing units of the original SLM and ISLMs are compared with the numerical analysis results of the staggered herringbone mixer (SHM) and barrier embedded micromixer (BEM) from Kang and Kwon's work (2004). Normalized mixing entropy ( $\kappa$ ) is represented as (Kang and Kwon 2004):

$$\kappa = \frac{S - S_0}{S_{\max} - S_0} \quad (6)$$

where  $S_0$  is the initial mixing entropy, which is zero, and  $S_{\max}$  is the maximum mixing entropy ( $\ln N_s$  as mentioned above).

#### 4 Experimental

Mixing experiment was performed with the original SLM and ISLMs for comparison purpose. Each micromixer was fabricated by polydimethylsiloxane (PDMS) (Duffy et al. 1998; Jo et al. 2000). For the purpose of mixing visualization, phenolphthalein and NaOH solutions were injected into the microchannel via the two inlets, respectively (Liu et al. 2000; Kim et al. 2004, 2005). Normalized purple color intensity change of the phenolphthalein along the downchannel was evaluated to measure the mixing performance quantitatively (Kim et al. 2004, 2005). Three different  $Re$  of 0.2, 2 and 20 were considered in order to investigate the effect of  $Re$  on the mixing performance. The details of experiments are described below.

Figure 4 illustrates the fabrication process of the micromixer. A negative photoresist, SU-8 50 (MicroChem Corp., USA), was spin coated on a silicon wafer at a spin speed of 1,800 rpm for 30 s. Then, pre-baking at 65°C for 8 min and soft baking at 95°C for 25 min on the hot plate followed. After UV exposure with a dose of 250 mJ/cm<sup>2</sup>, post exposure baking was carried out at 65°C for 5 min and 95°C for 15 min on the hot plate. SU-8 was developed by SU-8 Developer (MicroChem Corp., USA) for 1 h at room temperature and rinsed by isopropyl alcohol (IPA).

Prepolymer of PDMS (Sylgard 184), mixed with a curing agent, was poured on the SU-8 patterned master and cured in the convection oven at 65°C for 6 h. Replicated PDMS layers (upper and lower layers) were peeled off carefully from the masters. Then, through holes for the inlets and the outlet were punched out on the upper layer of the micromixer with a tool of diameter of 2 mm. Finally, surface oxidation of PDMS replicas was carried out by plasma discharge, then, upper and lower layer were bonded with a proper alignment (Duffy et al. 1998).

By using a syringe pump (KDS200, KD Scientific Inc.), two solutions of 0.31 mol/L phenolphthalein and 0.33 mol/L NaOH dissolved in 99% ethanol were injected into two inlets, respectively, and flowed through the micromixer via T-junction (Liu et al. 2000; Kim et al. 2004, 2005). As a result of the rapid reaction between phenolphthalein and NaOH (Caldin 1964), the interface between two streams turns purple within a negligible time (of the order of 10<sup>-9</sup> s) compared to the characteristic mixing time (of the order of 10<sup>-1</sup>–10<sup>0</sup> s for the present micromixers' cases depending on  $Re$ ), from which one can visualize the mixing performance through the downchannel of micromixers. Optical microscope (OSM-1, DONGWON EnC Corp.) equipped with a CCD camera (TDI DigiCAM, Techsan Corp.) and an illumination lamp was set up right above the micromixer to capture the images of the mixing performance during experiments. Captured digital image provides the color intensity data per pixel, from which one can evaluate the mixing performance quantitatively (Kim et al. 2004, 2005). Twelve positions with adjacent

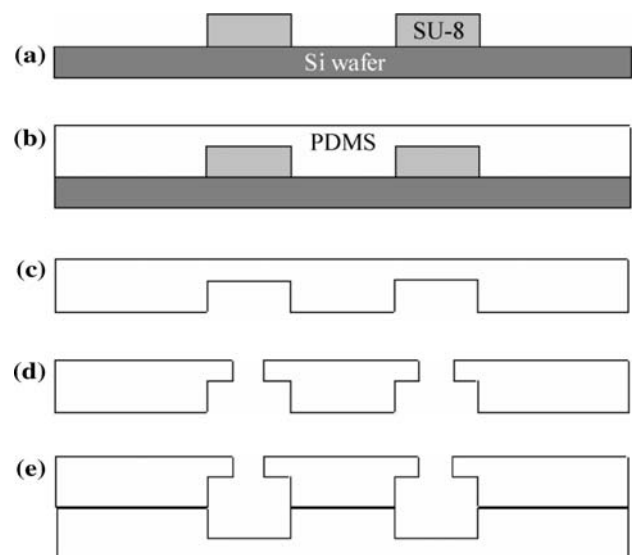
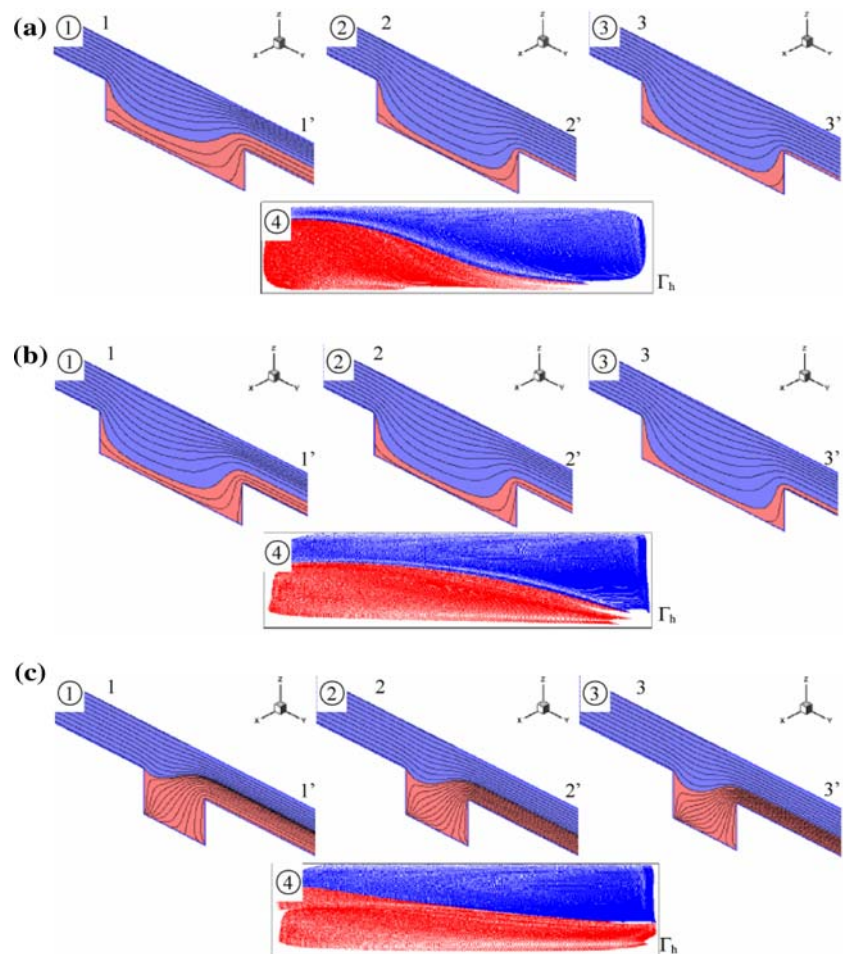


**Fig. 4** Fabrication process of the micromixer, **a** SU-8 patterning on the silicon wafer by UV photolithography, **b** PDMS casting on the SU-8 patterned master, **c** peeling off PDMS layer from the master, **d** punching holes for the inlets and the outlet, **e** bonding the two (upper and lower) layers of the PDMS after oxygen plasma treatment

**Fig. 5** Streamlines in the cross-sections at the recombination region (1–1', 2–2' and 3–3' depicted in Fig. 3) and colored particle distribution in the cross-sections  $\Gamma_h$  (depicted in Fig. 3) after 1 half period in the cases of **a** original SLM, **b** NDI ISLM and **c** NDII ISLM at  $Re = 0.2$



reference positions to compensate unwanted inhomogeneous illumination were selected along the downchannel direction for evaluation of mixing intensity (Kim et al. 2005). Normalized mixing intensity ( $\bar{I}$ ), adopted in the present study, is represented by Eq. 7 where  $n$ ,  $I_n$  and  $N$  is index for pixel, color intensity of pixel  $n$  and total number of pixels, respectively (Kim et al. 2005).  $\bar{I}_{ref}$  is a mean color intensity at the reference position,  $I_{max}$  is a maximum color intensity near the outlet introduced to normalize the mixing intensity.

$$\bar{I} = \frac{\sum_{n=1}^N I_n / N - \bar{I}_{ref}}{I_{max} - \bar{I}_{ref}} \quad (7)$$

## 5 Results and discussion

### 5.1 Numerical analysis result

This section describes (1) qualitative investigation on mixing behaviors of several designs of SLM, (2) the inertia effect on the mixing, and (3) quantitative evaluation of mixing performance in terms of mixing entropy.

It would be of great importance to understand how the vertical lamination takes place in the recombination region. Therefore, the streamlines in the cross-section of the recombination region, where two split streams (the first and second split streams in Fig. 2a) merge together, would help visualization of the vertical lamination characteristics. Figure 5 shows not only such streamlines (①, ② and ③) at three vertical cross-sections but also the consequence of vertical lamination mechanism after 1 half period of the mixing unit (④), for the cases of SLM (Fig. 5a) and NDI ISLM (Fig. 5b) and NDII ISLM (Fig. 5c). It might be mentioned that, red and blue colored particles are initially positioned at the left and right half in  $\Gamma_{in}$  (described in Fig. 3a), respectively. Thus, the first and second split streams are filled with blue and red particles as illustrated in Fig. 3a. The first and second split streams are supposed to be laminated in the upper and bottom layer, respectively, as in ④ in Fig. 5. It might be mentioned that complete vertical lamination (as indicated in Fig. 1b) is achieved only when the bottom layer would be perfectly laid under the upper one after the recombination. The recombination behavior of the original SLM turns out to be not so

good to realize such an ideal vertical lamination. In other words, streamlines in the three cross-sections are not uniformly developed (①, ② and ③ of Fig. 5a); two streams merge almost equally at the cross-section 1–1' while the upper stream prevails over the lower stream at the cross-sections 2–2' and 3–3'. Therefore, desirable vertical lamination with uniform lamella thickness is not accomplished, resulting in a rather diagonal-like lamination, as indicated in Fig. 5a④; red colored particles dominate left side of the cross-section while blue colored particles dominate right side. In the case of NDI ISLM, however, two streams merge in a more uniform fashion than the original SLM (①, ② and ③ of Fig. 5b); colored particle distribution clearly shows more uniformly achieved vertical lamination pattern of the NDI ISLM as shown in Fig. 5b④. In contrast, NDII ISLM develops the most desirable recombination behavior among the three designs; two streams are combined almost equally over the recombination region (①, ② and ③ of Fig. 5c), resulting in much better vertical lamination, as obviously shown in Fig. 5c④. The best vertical lamination of NDII ISLM is due to the significant upward motion in the lower channel as shown in Fig. 5c①, ② and ③. This is exactly how the design of NDII ISLM is inspired.

Shown in Fig. 6 are cross-sectional colored particle distributions after five successive mixing units of each design at  $Re = 20$ . Due to enhanced vertical lamination performance of the ISLMs, as discussed above, clearer lamella configurations can be observed in the ISLMs (Fig. 6b, c) than the original SLM (Fig. 6a); NDII ISLM accomplishes the most obvious lamellas of alternating colors. It may be mentioned that such successively developed lamella configurations, although their thicknesses are not perfectly uniform, can remarkably increase the interfacial area of two species.

It was demonstrated by the experiment of Liu et al. (2000) that the three-dimensional serpentine microchannel could induce the significant stirring effect as  $Re$  increases. In the present study, three-dimensional secondary flow due to the inertia effect is observed by numerical analysis of the original SLM and ISLMs in which serpentine geometry is also utilized. Flow analysis results at  $Re$  of 50 are considered for the purpose of illustrating secondary flow effect. For the case of  $Re = 50$ , Fig. 7a shows two-dimensional streamlines in four vertical cross-sections of the serpentine region  $\Omega_s$  (depicted in Fig. 3a). In these two-dimensional streamlines, secondary flow (i.e., a so-called vortex flow) is observed at the corner of the serpentine geometry. A single particle which happens to enter such a vortex region flows in the longitudinal direction of  $y$ -coordinate (depicted in Fig. 7) together with a rotational motion (in  $x-z$  plane) due to vortex-looking secondary flow, and then eventually exits the serpentine region, as illustrated by a three-dimensional trajectory in Fig. 7a. Precisely speaking, complex three-dimensional swirling flow is generated along the direction of  $y$ -coordinate with the vortex effect in  $x-z$  plane. When  $Re = 20$ , similar swirling flow with reduced strength is generated, while in the laminar flow regime, i.e., when  $Re = 0.2$ , no such swirling flow is observed due to insufficient advection effect, as presented in Fig. 7b where there is no vortex streamlines unlike Fig. 7a: the three-dimensional secondary flow effect of serpentine-type micromixers become effective for high  $Re$  regime. The swirling flow alone will result in a stretching effect only, thus existence of chaotic mixing may not be assured. However, periodic swirling flow followed by continuous splitting/recombination will give rise to the stretching and folding mechanism which is typical of chaotic mixing. In this respect, combined mixing

**Fig. 6** Cross-sectional colored particle distributions of the a original SLM, b NDI and c NDII ISLM at  $Re = 20$  for five periods

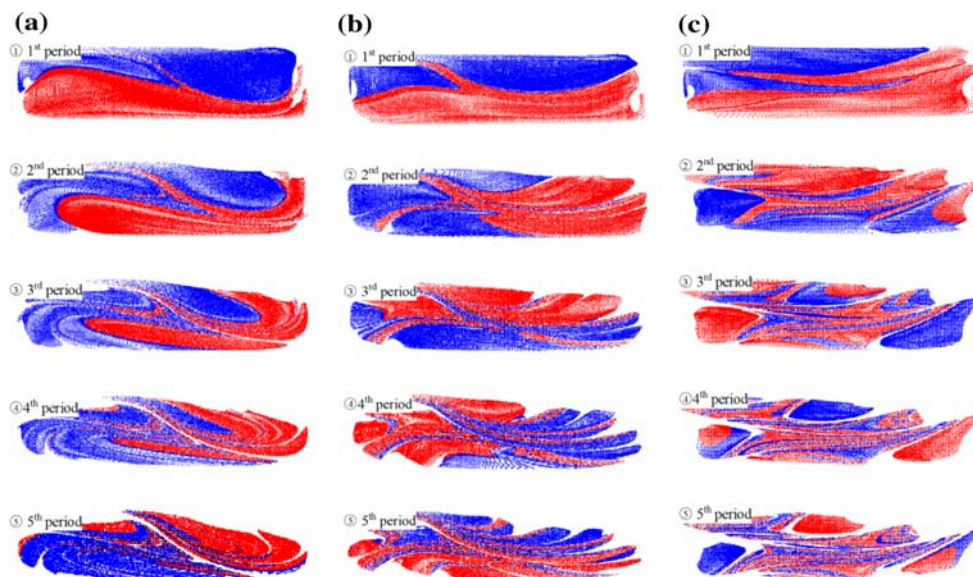




**Fig. 7** Streamlines with a trajectory of single particle at the serpentine corner region  $\Omega_s$  (depicted in Fig. 3) of the original SLM at **a**  $Re = 50$  and **b**  $Re = 0.2$

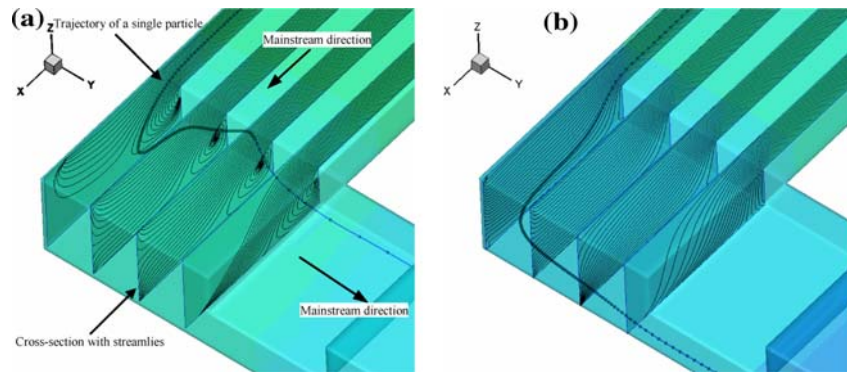
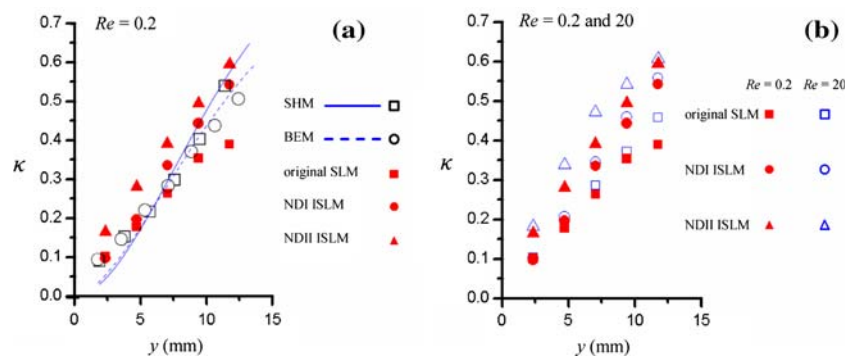


**Fig. 8** Mixing entropy changes of the original SLM and ISLMs along downchannel direction, **a** result at  $Re = 0.2$  for three designs of the present study and same analysis result of the SHM and BEM from Kang and Kwon's work, **b** result at  $Re = 0.2$  and 20 of three designs showing the inertia effect on mixing performance



mechanism of the SLM and ISLMs can favorably work out for chaotic mixing. It may be just noted that flow characteristics of ISLMs are almost the same as SLM in the serpentine region, thus no corresponding figures are being provided in this article.

Now, let us change our attention from qualitative investigation to quantitative mixing characteristics of these designs. Normalized mixing entropy ( $\kappa$ ), defined in Eq. 6, was calculated up to five mixing units (equivalent to 11.75 mm in downchannel direction). Figure 8 shows how the normalized mixing entropy increases with downchannel direction in the case of original SLM and ISLMs. For the case of low  $Re$  regime, Kang and Kwon (2004) reported the same mixing analysis with no inertia effect for staggered herringbone mixer (SHM) and barrier embedded micromixer (BEM), that are also plotted in Fig. 8a, for a comparison purpose. Figure 8a shows that NDII ISLM achieves the most efficient mixing among the five micromixers; mixing performance of NDI ISLM is close to the SHM; the original SLM achieves a slightly lower mixing performance than the BEM. Plotted in Fig. 8b are the normalized mixing entropy behavior of three designs for the case of  $Re = 20$ , clearly indicating higher mixing performance compared with the low  $Re$  case, obviously due to the inertia effect described by the swirling flow in the serpentine region. This result suggests that three-dimensional secondary flows in the serpentine region due to

inertia effect can favorably work out to improve the mixing performance by enhancing the stretching and folding of the fluid elements as  $Re$  increases.

## 5.2 Experimental verification

In this section, (1) lamination performance of each design is compared, in a qualitative manner, via flow visualization with the help of color change in the interface surface between two liquids and (2) mixing performance is verified quantitatively by means of normalized mixing intensity.

Figure 9 presents optical micrographs (top-view) of the micromixers showing the color change (from transparent to purple) in the interface surface, together with magnified images at the first mixing unit, for each design in a steady state at  $Re = 2$ . Since purple interface behavior can be easily identified in the first mixing unit, vertical lamination performance is more closely observed, at first, by tracing the purple interface in a magnified image of the first mixing unit. In a magnified image, the interface at the T-junction is vertical and thus seen as just a line. The interface surface deforms along the downchannel direction and tends to become horizontal at the first recombination region. For the ideal vertical lamination case, it will be lying in a perfectly horizontal plane as depicted in Fig. 1bD. As mentioned in the previous section of numerical analysis, the interface



after the first recombination region is located in an almost diagonal direction (Fig. 5aⒺ) in the case of SLM, while those of NDI and NDII ISLMs tend to rotate to a horizontal plane (Fig. 5bⒺ and cⒺ). Particularly for the case of original SLM, the interface is not fully extended to the whole cross section ( $\Gamma_h$  in Fig. 3) and therefore, the interface would have a boundary in the plan view (Fig. 9a) in such an incomplete vertical lamination. In this regard, the boundary of the purple interface is highlighted by blue curves in Fig. 9. In Fig. 9b, blue boundary curve of NDI ISLM is also located along the second split stream, however, it is closer to the channel wall than the original SLM due to more uniform vertical lamination performance of NDI ISLM as shown by Fig. 5bⒺ. In contrast, there is no such blue boundary curve in the case of NDII ISLM (Fig. 9c) since the interface is fully extended to cover the entire cross section, as indicated in Fig. 5cⒺ. In this respect, this experimental visualization result is consistent with the numerical analysis.

Figure 10 shows the normalized mixing intensity versus downchannel location for several  $Re$  cases. Optimal fitting curves, in this figure, are obtained by using equation:

$$\bar{I} = 1 - \exp(-\gamma/\gamma) \tag{8}$$

where  $y$  and  $\gamma$  are the downchannel location and the characteristic required mixing length, respectively (Kim et al. 2005). It may be mentioned that the shorter the characteristic required mixing length, the better the mixing was achieved. The mixing performances of ISLMs, as expected, are significantly improved; NDII ISLM accomplishes the most efficient mixing performance among the three designs. Averaged value of  $\gamma$  for those three  $Re$  cases of NDI and NDII ISLMs are 4.97 and

3.89 mm, respectively, which is about 1.3 and 1.6 times shorter than that of the original SLMs of 6.32 mm. It may be mentioned that mixing intensity in Fig. 10 generally decreases as  $Re$  increases. However, one should note that the residence time decreases as  $Re$  increases, thus more diffusion effect is considered in the results of lower  $Re$  case of Fig. 10. Therefore, direct observation of  $Re$  effect on the mixing performance would be complicated from Fig. 10. In this regard, we modify Eq. 8 with an assumption of  $y(t) = Vt$  where  $V$  is the characteristic velocity. Then one obtains the following relation between mixing intensity and time:

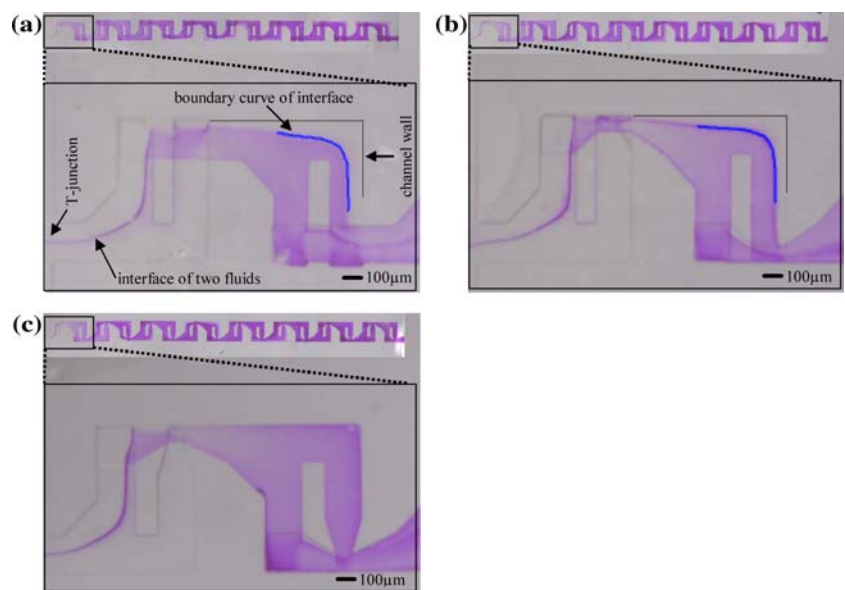
$$\bar{I} = 1 - \exp(-Vt/\gamma) = 1 - \exp(-t/\theta) \tag{9}$$

where  $\theta = \gamma/V$  can be referred to as a “characteristic required residence time”. Physically,  $\theta$  represents residence time when  $\bar{I}$  reaches 0.632 from zero. In Table 1, characteristic required mixing length ( $\gamma$ ) and residence time ( $\theta$ ) of the SLM and ISLMs are shown for several  $Re$ . If mixing is achieved only by diffusion (for example, mixing within a simple T-channel in a laminar flow regime) then the order of magnitude of  $\theta$  can be predicted by Fick’s law as:

$$\theta \sim d^2/D \tag{10}$$

where  $d$  and  $D$  are the length scale of lamellae and diffusion coefficient, respectively. In this case, theoretically,  $\theta$  remains the same (order of several min if  $d$  of 100  $\mu\text{m}$  and  $D$  of  $10^{-10} \text{ m}^2/\text{s}$  are considered) irrespective of  $Re$ , thus  $\gamma$  increases linearly as  $Re$  increases. In contrast, for the cases of SLM and ISLMs in Table 1, it turns out that  $\theta$  decreases as  $Re$  increases, and therefore,  $\gamma$  remains in the order of few mm even at the high  $Re$  of 20. In this regard, it can be

**Fig. 9** Mixing experimental results and enlarged microscopic views of first mixing units for the **a** original SLM, **b** NDI and **c** NDII ISLM at  $Re$  of 2. Vertical lamination patterns are shown by purple interface of two fluids. The blue curve in the figures indicates the boundary of the purple interface



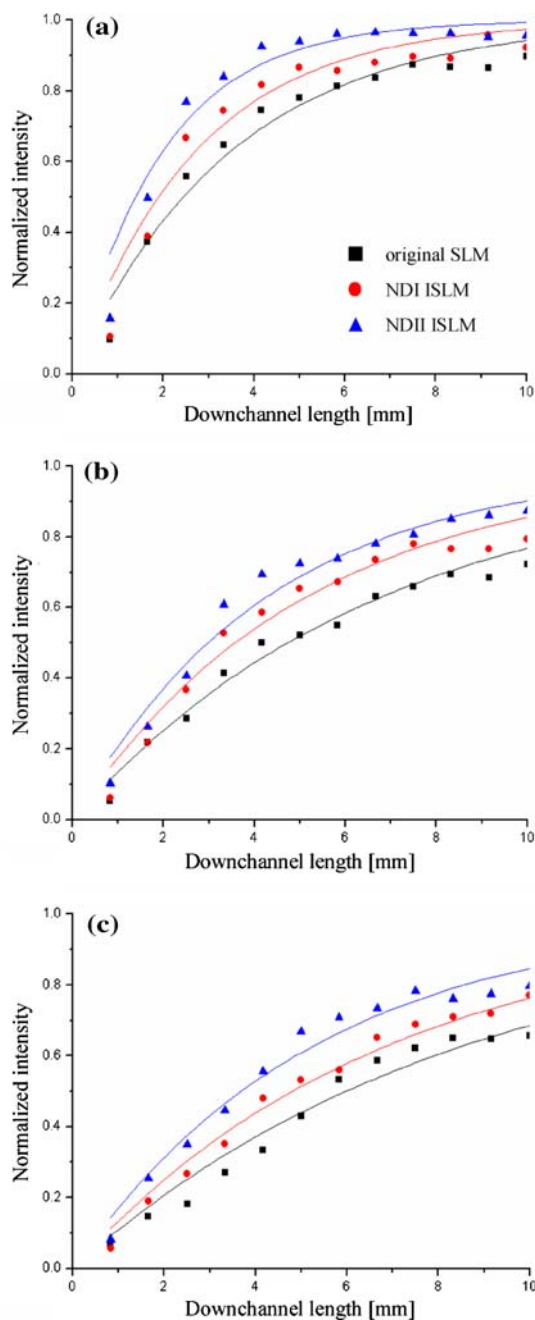


**Fig. 10** Normalized mixing intensity changes along downchannel direction of the SLMs at  $Re$  of **a** 0.2, **b** 2 and **c** 20. Symbols: experimental data and curves: optimal fitting by Eq. 8. Characteristic required mixing lengths, i.e.  $\gamma$ , of the original SLM are 3.54, 6.81 and 8.60 mm, respectively to the  $Re$  of 0.2, 2 and 20, while NDI ISLM achieves 2.77, 5.18 and 6.97 mm and NDII ISLM achieves 2.00, 4.33 and 5.34 mm

mentioned that mixing mechanisms of SLM and ISLMs become more effective as  $Re$  increases, consequently maintaining  $\gamma$  within a mm scale; one has also seen from numerical analysis results that the mixing performances of SLM and ISLM get better as  $Re$  increases in terms of mixing entropy.

**Table 1** Characteristic required mixing length and residence time of SLM and ISLMs for several  $Re$

	$Re = 0.2$	$Re = 2$	$Re = 20$
$\gamma$ (mm)			
SLM	3.54	6.82	8.60
NDI ISLM	2.77	5.18	6.97
NDII ISLM	2.00	4.33	5.34
$\theta$ (s)			
SLM	7.27	1.40	0.18
NDI ISLM	5.69	1.06	0.14
NDII ISLM	4.46	0.89	0.11

Finally, it should be noted that the present experimental results agree with the numerical analysis results in the respect that: (1) mixing performances of ISLMs are enhanced over the SLM, and NDII ISLM achieves the best; (2) mixing mechanisms of SLM and ISLMs become more effective as  $Re$  increases.

## 6 Conclusion

The present study reports that mixing performance of SLM could be further improved by “simple” geometric redesign of the original “F”-shape mixing unit in such a way that enhanced local advection helps better vertical lamination. Two designs (NDI and NDII) of improved SLM (ISLM) were proposed. The flow characteristics and mixing performances of the original and improved SLMs were investigated numerically and verified experimentally.

Numerical analysis system was developed based on the finite element method and colored particle tracking method. By means of streamlines at the recombination region and colored particle distribution after one half period, it was shown that NDI and NDII drive two split streams into more efficient vertical lamination than the original design; NDII ISLM achieves the most efficient vertical lamination among three designs. In addition, three-dimensional swirling flow was observed at the corner of the serpentine region when  $Re \gg 1$ , eventually enhancing the mixing performance by generating the stirring effect. Mixing entropy results confirmed mixing enhancement of the ISLMs; NDII ISLM achieved most efficient chaotic mixing among the five micromixers (SHM, BEM, SLM and two ISLMs).

The mixing experiment was conducted with SLM and ISLMs which were realized by PDMS casting. Phenolphthalein and NaOH solutions were utilized for visualization of mixing performance. Optical micrograph of the first mixing unit clearly showed that NDII ISLM achieves the most efficient vertical lamination among the

three designs. Normalized mixing intensity change along the downchannel confirmed highly enhanced mixing performance of ISLMs, which is consistent with numerical analysis result; NDII ISLM performs the best mixing among the three designs.

**Acknowledgments** The authors would like to thank the Korean Ministry of Commerce, Industry and Energy for financial support via the Development of Next-Generation New Technology Program and Korean Ministry of Education and Human Resources Development supporting BK21 program.

## References

- Aref H, Balachandar S (1986) Chaotic advection in a Stokes flow. *Phys Fluids* 29:3515–3521
- Branebjerg J, Gravesen P, Krog JP, Nielsen CR (1996) Fast mixing by lamination. *Proceedings of the IEEE micro electro mechanical systems*, pp 441–446, San Diego
- Byrde O, Sawley ML (1999) Optimization of a Kenics static mixer for non-creeping flow condition. *Chem Eng J* 72:163–169
- Caldin EF (1964) *Fast reactions in solution*. Wiley, New York
- Camesasca M, Manas-Zloczower I, Kaufman M (2005) Entropic characterization of mixing in microchannels. *J Micromech Microeng* 15:2038–2044
- Chow AW (2002) Lab-on-a-chip: opportunities for chemical engineering. *AIChE J* 48:1590–1595
- Duffy DC, McDonald JC, Schueller OJA, Whitesides GM (1998) Rapid prototyping of microfluidic systems in poly(dimethylsiloxane). *Anal Chem* 70:4974–4984
- Franca LP, Frey SL (1992) Stabilized finite element methods: II. The incompressible Navier–Stokes equations. *Comput Methods Appl Mech Eng* 99:209–233
- Hughes TJR, Franca LP, Hulbert GH (1989) A new finite element formulation for computational fluid dynamics: VIII. The Galerkin/least-squares method for advective–diffusion equations. *Comput Methods Appl Mech Eng* 188:235–255
- Hwang WR, Kwon TH (2000) Dynamical modeling of chaos single-screw extruder and its three-dimensional numerical analysis. *Polym Eng Sci* 40:702–714
- Jo B-H, Lerberghe LMV, Motsegood KM, Beebe DJ (2000) Three-dimensional micro-channel fabrication in polydimethylsiloxane (PDMS) elastomer. *J Microelectromech Syst* 9:76–81
- Kang TG, Kwon TH (2004) Colored particle tracking method for mixing analysis of chaotic micromixers. *J Micromech Microeng* 14:891–899
- Kim SJ, Kwon TH (1996) Enhancement of mixing performance of single screw extrusion process via chaotic flows. *Adv Polym Tech* 15:41–69
- Kim DS, Lee SW, Kwon TH, Lee SS (2004) A barrier embedded chaotic micromixer. *J Micromech Microeng* 14:798–805
- Kim DS, Lee SH, Kwon TH, Ahn CH (2005) A serpentine laminating micromixer combining splitting/recombination and advection. *Lab Chip* 5:739–747
- Kim DS, Lee SH, Ahn CH, Lee JY, Kwon TH (2006) Disposable integrated microfluidic biochip for blood typing by plastic microinjection moulding. *Lab Chip* 6:794–802
- Lee Y-K, Deval J, Tabeling P, Ho C-H (2001) Chaotic mixing in electrokinetically and pressure driven micro flows. *Proceedings of the IEEE micro electro mechanical systems*, pp 483–486, Interlaken
- Liu RH, Stremler MA, Sharp KV, Olsen MG, Santiago JG, Adrian RJ, Aref H, Beebe DJ (2000) Passive mixing in a three-dimensional serpentine microchannel. *J Microelectromech Syst* 9:190–197
- Manz A, Grabber N, Widmer HM (1990) Miniaturized total chemical analysis systems: a novel concept for chemical sensing. *Sens Actuators B* 1:244–248
- Ottino JM (1989) *The kinematics of mixing: stretching, chaos and transport*. Cambridge University Press, New York
- Schönfeld F, Hessel V, Hofmann C (2004) An optimized split-and-recombine micro-mixer with uniform ‘chaotic’ mixing. *Lab Chip* 4:65–69
- Schwesinger N, Frank T, Wurmus H (1996) A modular microfluid system with an integrated micromixer. *J Micromech Microeng* 6:99–102
- Stroock AD, Dertinger SKW, Ajdari A, Mezić I, Stone HA, Whitesides GM (2002) Chaotic mixer for microchannels. *Science* 295:647–651
- Verpoorte E (2002) Microfluidic chips for clinical and forensic analysis. *Electrophoresis* 23:677–712